symmetry

MDPI

Article

Response-Tunable Adaptive LOS-Based Guidance for Depth-Tracking Control of Underactuated AUVs in the Presence of Time-Varying Disturbances

Xinyu Li [1], Gang Wan [1], Sisi Zhu [1], Changxing Nie [2], Weijian Huang [2], Zhiyuan Yin [2] and Yang Qu [2,*]

[1] Hubei Technology Innovation Center for Smart Hydropower, Wuhan 430019, China
[2] School of Naval Architecture and Ocean Engineering, Huazhong University of Science and Technology, Wuhan 430074, China
* Correspondence: yangqu@hust.edu.cn

Abstract

Autonomous underwater vehicles (AUVs) have been extensively employed in diverse marine applications, where depth-tracking control remains a critical technical challenge. Although previous studies have investigated various guidance law designs for underactuated AUVs, compensation for the attack-angle effect induced by heave velocity remains underexplored, particularly in the presence of extreme time-varying external disturbances and sharp path curvature variations. Existing line-of-sight (LOS) based methods, including integral LOS (ILOS) and adaptive LOS (ALOS), rely solely on the integral action of the pitch-tracking error to estimate the attack angle, which inevitably introduces inherent time-delay characteristics and induces overshoot and chattering in the depth-tracking response. Given that a system's position and its velocity are uniquely determined by its acceleration, a response-tunable adaptive LOS (RTALOS) guidance design is proposed for AUV depth-tracking control task. This guidance law incorporates both the depth-tracking error and its velocity term as boundary constraints, generating an acceleration reference through a time-based planning polynomial to achieve accurate attack-angle estimation. The proposed method redefines attack-angle estimation as a new paradigm based on a second-order depth-tracking kinematic system, where the introduced velocity term acts as an adjustable damping effect to effectively suppress the depth-tracking overshoot and oscillation. Simulations were conducted to verify that the proposed guidance design could make the depth-tracking motion converge within a given time duration if the state-constrained acceleration was promptly executed. Compared to the selected ILOS and ALOS methods, the proposed RTALOS method can rapidly and accurately compensate for time-varying attack-angle effects via the estimation of attack angle, resulting in precise depth-tracking control performance, even under severe time-varying disturbances and when the pitch-tracking control performance is unsatisfactory.

Keywords: adaptive LOS-based guidance; response-tunable convergence; depth-tracking control; time-varying disturbances; underactuated AUVs

Check for updates

Academic Editor: Vasilis K. Oikonomou

Received: 11 September 2026
Revised: 1 October 2026
Accepted: 5 October 2026
Published: 16 October 2026

Copyright: © 2026 by the authors. Licensee MDPI, Basel, Switzerland. This article is an open access article distributed under the terms and conditions of the Creative Commons Attribution (CC BY) license.

1. Introduction

In recent decades, autonomous underwater vehicles (AUVs) have been extensively deployed in diverse marine missions, including scientific surveys, seabed resource exploration, bathymetric mapping, underwater structural inspection, salvage operations,

hydrographic investigation, and emergency search and rescue [1]. Unlike remotely operated vehicles, which rely on umbilical cables for power and data transmission, AUVs exhibit superior operational autonomy and broader mission coverage [2–6]. As deep-sea exploration expands and the demand for high-precision seabed operations increases, underactuated rudder-propeller-driven AUVs have gained substantial research attention. This interest stems from their advantages of low energy consumption, compact configuration, and high reliability. With the continuous expansion of deep-sea exploration and seabed precision operation demands, depth-tracking control remains a critical and persistently evolving technical challenge [7–13]. Under realistic ocean conditions, depth-control accuracy is degraded by multiple factors: complex time-varying currents, near-bottom effects induced by seabed topography, and physical limitations of the actuation system. These challenges have collectively motivated continuous advances in guidance-law design and disturbance-rejection strategies [14–16]. These disturbance-rejection requirements have also motivated observer-based robust control designs for uncertain nonlinear systems subject to multiple disturbances [17–21].

For underactuated AUV depth-tracking tasks, the main objective is to achieve pitch-angle guidance at the kinematic level and its tracking control at the kinetic level. Specifically, a mapping relationship between the depth-tracking error and the desired pitch angle needs to be established. This mapping serves as the design objective of the pitch-angle guidance law [22]. The desired pitch angle, generated by this guidance law, is subsequently delivered to the low-level pitch-angle controller for closed-loop tracking. Owing to the underactuated actuator configuration, the depth-tracking performance of the AUV is inevitably affected by nonlinear hydrodynamic characteristics and unknown environmental disturbances. As a classical guidance strategy, the line-of-sight (LOS) guidance method has been widely adopted in trajectory-tracking and path-following problems for marine vehicles in recent years [6,23–29]. To further improve depth-control accuracy, existing approaches typically incorporate an additional compensation angle into the guidance law to counteract the attack-angle effect induced by heave velocity [30,31]. The primary difficulty in this process lies in the accurate estimation and effective compensation of the attack angle. Moreover, the time-varying characteristics of the attack angle are strongly coupled with complex external load conditions and the path curvature.

Within the LOS guidance framework, how to incorporate an additional compensation angle into the guidance law has become a core difficulty in guidance design. For horizontal-plane tracking control, this compensation angle corresponds to the sideslip-angle compensation [23,32,33]. For depth-tracking problems, it corresponds to the attack-angle compensation [17,22]. Current research mainly follows two technical approaches to estimate this compensation angle. The first approach involves designing an observer that treats the compensation angle as one of its state outputs and indirectly estimates the attack or sideslip angle using the integral of the tracking error. The second approach directly introduces an integral term of the tracking error to achieve online estimation and compensation. The general form of the pitch-angle guidance law considering attack-angle compensation consists of a path azimuth angle, a fixed-gain term related to the depth-tracking error, and two integral correction terms. These two integral terms distinguish the adaptive LOS (ALOS) guidance from the integral LOS (ILOS) guidance. A clear distinction between the two is provided in [34]. The ALOS guidance retains only the first integral correction term, whereas ILOS guidance retains only the second one. In terms of specific implementations, ref. [35] proposed an improved adaptive LOS guidance law based on two extended state observers that estimate surge and sway linear velocities, thereby achieving attack-angle compensation. In [36–38], different types of nonlinear observers were designed for attack-angle estimation, and LOS guidance laws with attack-angle or sideslip-angle compensation

were accordingly constructed. Furthermore, refs. [29,34,39–42] proposed different types of ILOS guidance laws that utilize the integral effect of the tracking error to estimate the attack-angle or sideslip-angle angle. In contrast, refs. [27,34,41] proposed various ALOS guidance laws, which are typically characterized by employing an independent adaptive integral term to estimate the attack angle separately. A qualitative comparison of these LOS-based guidance methods is summarized in Table 1.

In recent years, researchers have developed various improved strategies based on the LOS guidance framework, including multi-LOS fusion, predictive LOS, and virtual-reference-point guidance, to meet the control demands in complex curved paths and strong-disturbance marine environments [17]. For the three-loop cascaded system consisting of state estimation, pitch-angle guidance, and pitch-angle control, ref. [22] proposed a cascaded architecture with temporal-convergence characteristics. In this architecture, the state-estimation loop is required to converge first, followed by the control-execution loop and finally the guidance-regulation loop. Their study also indicated that the mismatch of convergence rates among the three loops is a key factor inducing system oscillation. In addition, to address practical engineering issues such as model parameter uncertainties and unmeasurable state variables, domestic researchers have conducted a series of studies on time-based control strategies and output-feedback schemes. These efforts provide useful references for enhancing the robustness of depth-tracking systems [43,44]. Nevertheless, most existing methods are built upon the assumption that the attack angle slowly varies with small amplitude. Moreover, the estimation of the guidance compensation angle relies only on the integral action of the tracking error [29,34]. Consequently, their applicability is mainly limited to tracking tasks under slowly varying environmental disturbances and paths with small curvature. When the path curvature changes sharply or sudden environmental load variations occur, the vehicle may experience significant sideslip effects. Meanwhile, the inherent time-delay characteristics of the integral action can further induce overshoot and chattering, severely degrading the tracking accuracy and stability of the system [22]. It is worth noting that the vast majority of current time-based convergence designs remain confined to the dynamic control layer. The response-tunable guidance theory oriented toward sideslip-angle estimation still requires further development.

When the predefined path curvature changes sharply or sudden environmental disturbances occur, the existing strategies that rely solely on the integral of the tracking error for guidance-angle estimation will expose the inherent time-delay characteristics of the integral action, thereby inducing overshoot and chattering in the tracking system. To address the above issues, this paper proposes a response-tunable adaptive LOS (RTALOS) guidance design for the depth-tracking control of underactuated AUVs. In the guidance-angle estimation process, the proposed RTALOS guidance incorporates not only the depth-tracking error but also its velocity term. This velocity term can provide additional damping effect to the tracking-error system, thereby effectively suppressing overshoot and chattering. In terms of specific implementation, the proposed RTALOS guidance takes the depth-tracking error and its velocity as boundary constraints, generates an acceleration reference through a time-based planning polynomial, and then completes the attack-angle estimation accordingly. Consequently, the depth-tracking guidance system possesses response-tunable convergence characteristics. For the depth-tracking control problem of underactuated AUVs, the main contributions of this paper are summarized in the following three aspects:

1. Unlike existing ILOS and ALOS methods that rely solely on the integral action of the cross-tracking error to estimate the attack angle or the sideslip angle [17,23,34,35,37,39–42,45], this paper proposes a novel response-tunable guidance method, namely RTALOS, which is built upon a state-constrained time-based planning polynomial. Different from the conventional integral-action-based estimation, the proposed method redefines the

attack-angle estimation as a new paradigm that simultaneously incorporates the cross-tracking error and its velocity term, thereby achieving fast and accurate attack-angle estimation without introducing additional integral lag.

2. Existing ILOS and ALOS methods are typically derived from a first-order cross-tracking kinematic model to obtain the attack-angle or sideslip-angle update law [17,23,34,35,37,39–42,45]. In contrast, the proposed RTALOS guidance method is developed from a second-order cross-tracking kinematic system, which provides an additional degree of freedom for shaping the transient response. In particular, the cross-tracking velocity term introduced in the attack-angle estimation acts as an adjustable damping term for this second-order tracking system, and the convergence rate can be directly tuned through the planning-time parameter. As a result, the overshoot and oscillation problems inherent in conventional pure-integral strategies are effectively suppressed.
3. To validate the effectiveness of the proposed RTALOS guidance method, a response-tunable pitch-tracking controller is further proposed to accurately track the desired pitch angle generated by the RTALOS guidance. In addition, PD control, active disturbance rejection control (ADRC), and the proposed response-tunable control are respectively combined with the ILOS, ALOS, and RTALOS guidance laws to form multiple comparative groups. Comparative simulations are conducted under strong time-varying disturbance conditions, and the performance is evaluated by multiple quantitative indices. The results demonstrate that, compared with ILOS and ALOS, the proposed RTALOS method can accurately estimate the time-varying attack angle, which is jointly affected by time-varying loads and pitch-angle control deviations, even when the PD control performance is unsatisfactory. Consequently, the proposed method achieves significantly superior depth-tracking control performance.

The remainder of this paper is organized as follows. Section 2 presents the mathematical model of the AUV depth-tracking task and formulates the depth-tracking control problem. Section 3 introduces a uniformed model transformation to derive the second-order depth-tracking kinematics and pitch-tracking dynamics. Section 4 presents the uniformed state-constrained response-tunable guidance and controller design. Section 5 provides simulation analysis and validation results. Section 6 concludes the paper.

Table 1. Comparisons of existing LOS-based guidance methods.

Method	References	Sideslip Angle	Main Characteristics
LOS	[46]	Neglected	Simple structure, but the tracking error is relatively large when the sideslip angle is non-negligible.
ILOS	[23,40,45]	Compensated by the integral of the tracking error	Relies on the small-sideslip-angle assumption; the integral action introduces time lag, which may cause overshoot and oscillation.
ALOS	[34,39,41,42]	Estimated by an integral term of the tracking error	Suffers from the inevitable time-delay characteristics, leading to overshoot and oscillation in the tracking response.
ELOS	[35–38]	Estimated by a designed observer	Achieves explicit sideslip-angle estimation, but the overall structure is more complex.

2. Preliminaries

2.1. AUV Mathematical Model

As illustrated in Figure 1, the mathematical modeling of an AUV is based on two primary reference frames: the inertial coordinate system $O_I - X_I Y_I Z_I$ (North-East-Down) and the body-fixed coordinate system $O_B - X_B Y_B Z_B$. For simplicity, the origin O_B is typically aligned with the vehicle's center of gravity. Following the standard formulations in [46], the kinematic and dynamic behavior of an AUV can be described as follows:

$$\dot{\boldsymbol{\eta}} = \boldsymbol{J}(\boldsymbol{\eta})\boldsymbol{v}, \tag{1}$$

$$\boldsymbol{M}\dot{\boldsymbol{v}} + \boldsymbol{C}(\boldsymbol{v})\boldsymbol{v} + \boldsymbol{D}(\boldsymbol{v})\boldsymbol{v} + \boldsymbol{g}(\boldsymbol{\eta}) = \boldsymbol{\tau} + \boldsymbol{d}, \tag{2}$$

where the vector $\boldsymbol{\eta} = [x, y, z, \phi, \theta, \psi]^{\mathrm{T}}$ defines the AUV's position and Euler angles in the inertial coordinate system $O_I - X_I Y_I Z_I$. The velocity components, including linear and angular rates, are represented by $\boldsymbol{v} = [u, v, w, p, q, r]^{\mathrm{T}}$ in the body-fixed coordinate system $O_B - X_B Y_B Z_B$. The mapping between these two frames is provided by the transformation matrix $\boldsymbol{J}(\boldsymbol{\eta})$. Regarding the dynamic Equation (2), $\boldsymbol{M}$ denotes the system's inertia matrix (comprising rigid-body and added mass effects), while $\boldsymbol{C}(\boldsymbol{v})$ and $\boldsymbol{D}(\boldsymbol{v})$ characterize the Coriolis-centripetal forces and hydrodynamic damping terms, respectively. The restoring force vector, arising from the balance of gravity and buoyancy, is represented by $\boldsymbol{g}(\boldsymbol{\eta})$. Furthermore, $\boldsymbol{\tau}$ and $\boldsymbol{d}$ denote the control input vector and the environmental disturbances, respectively. Detailed formulations of these matrices can be found in [46].

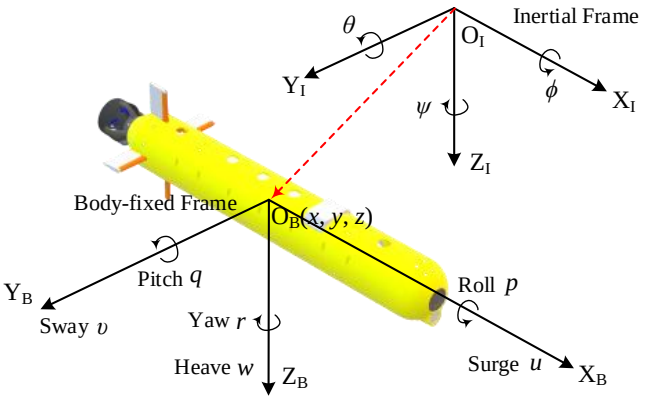


Figure 1. The coordinate systems defined for AUVs.

2.2. AUV Depth-Tracking Dynamic Model

For the depth-tracking control task, the maneuvering motions of the AUV in the vertical plane are considered, namely surge, heave, and pitch dynamics. In particular, a constant surge propulsion force is generated to make the AUV move forward. Consequently, this paper will focus on the heave and pitch dynamic models, which provides

$$\begin{aligned}(m - Z_{\dot{w}})\dot{w} - (Z_{\dot{q}} + mx_g)\dot{q} &= muq + (W - B)\cos(\theta) \\ &+ Z_{w|w|}w|w| + Z_{q|q|}q|q| + Z_{uq}uq \\ &+ Z_{uw}uw + Z_d + Z_{uu\delta_s}u^2\delta_s,\end{aligned} \tag{3}$$

$$\begin{aligned}(I_{yy} - M_{\dot{q}})\dot{q} - (M_{\dot{w}} + mx_g)\dot{w} &= z_b B\sin(\theta) \\ &+ M_{w|w|}w|w| + M_{q|q|}q|q| + M_{uq}uq \\ &+ M_{uw}uw + M_d + M_{uu\delta_s}u^2\delta_s,\end{aligned} \tag{4}$$

where θ denotes the vehicle's pitch angle, u gives its surge speed, and w and q represent the heave and pitch velocities, respectively. The gravity and buoyancy forces are denoted by

W and B, respectively. The hydrodynamic coefficients are given by $Z_{w|w|}$, $Z_{q|q|}$, Z_{uq}, Z_{uw}, $M_{w|w|}$, $M_{q|q|}$, M_{uq}, and M_{uw}. The environmental disturbance force and moment are Z_d and M_d, respectively. δ_s gives the AUV's elevator angle. The heave force and pitch moment generated by the elevator are expressed as $Z_{uu\delta_s}u^2\delta s$ and $Muu\delta_s u^2\delta_s$, respectively.

2.3. AUV Depth-Tracking Problem Formulation

The depth-tracking control problem for underactuated AUVs considers only the vehicle's motion in the vertical plane, namely the surge, heave, and pitch, as shown in Figure 2. For such an underactuated AUV, its control actuators can generate only a surge force and pitch moment, allowing the vehicle to move forward and rotate about its y-axis. To handle the underactuation problem, a state constraint that relates the depth-tracking error to the desired pitch angle should be introduced. This constraint, which effectively reduces the depth-tracking motion from three degrees of freedom (DOF) to two DOF, constitutes the guidance law design.

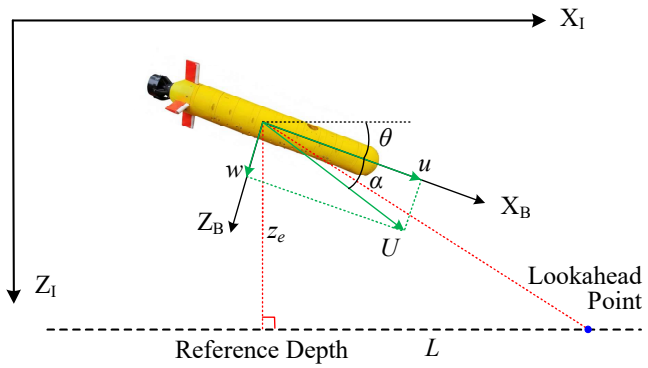


Figure 2. The depth-tracking guidance description for an underactuated AUV.

Based on the three DOF kinematic model in Equation (1), the depth-tracking kinematic model can be written as

$$\dot{z} = -u\sin(\theta) + w\cos(\theta) = U\sin(\alpha - \theta), \tag{5}$$

$$\dot{\theta} = q, \tag{6}$$

where z denotes the vehicle's depth. The cruise speed U in vertical plane is written as $U = \sqrt{u^2 + w^2}$. The attack angle α is formulated as $\alpha = \text{atan2}(w, u)$.

Let z_d denote the desired depth. The depth-tracking error z_e is defined as $z_e = z - z_d$. As shown in Figure 2, the LOS-based desired pitch angle can be derived as

$$\theta_d = \arctan\left(\frac{z_e}{L}\right) + \hat{\alpha}, \tag{7}$$

where parameter L represents the lookahead distance. $\hat{\alpha}$ gives an estimation of the attack angle.

In this context, the depth-tracking control problem can be specified into the following two categories:

1. *Pitch-tracking control execution*: The LOS-based guidance law generates a desired pitch angle θ_d as given in Equation (7). The pitch-tracking controller should therefore produce a series of control commands such that the vehicle's pitch angle θ can accurately follow the desired signal, i.e., $\theta \to \theta_d$.
2. *Accurate estimation of attack angle*: The sideslip effects encountered during depth tracking are primarily caused by the vehicle's attack angle α. To effectively compensate

for these sideslip effects, an update law for the estimated attack angle $\hat{\alpha}$ should be designed to improve the depth-tracking performance.

3. Uniformed Model Transformation

In this section, a uniformed second-order system is developed for both the pitch-tracking dynamic model and the depth-tracking kinematic model, enabling the application of a uniform control framework to both systems. This uniformed second-order system is described as

$$m_\zeta \ddot{\zeta} + d_\zeta = \tau, \tag{8}$$

where m_ζ represents a mass-like or moment-of-inertia-like gain parameter. $\ddot{\zeta}$ denotes the system acceleration. d_ζ lumps together all unknown nonlinearities and uncertainties. τ is the control input.

3.1. Transformed Pitch-Tracking Dynamic Model

We rewrite the heave and pitch dynamic models described in Equations (3) and (4) as follows:

$$(m - Z_{\dot{w}})\dot{w} - (Z_{\dot{q}} + mx_g)\dot{q} + d_w = Z_{uu\delta_s} u^2 \delta_s, \tag{9}$$

$$(I_{yy} - M_{\dot{q}})\dot{q} - (M_{\dot{w}} + mx_g)\dot{w} + d_q = M_{uu\delta_s} u^2 \delta_s, \tag{10}$$

where d_w and d_q are the corresponding nonlinear terms that lump all uncertainties together.

Inserting the heave dynamic model of Equation (9) into the pitch dynamic model of Equation (10) to replace the heave acceleration $\dot{w}$ yields

$$m_\theta \ddot{\theta} + d'_\theta = \delta_s, \tag{11}$$

where

$$m_\theta = \frac{(I_{yy} - M_{\dot{q}})(m - Z_{\dot{w}}) - (M_{\dot{w}} + mx_g)(Z_{\dot{q}} + mx_g)}{(M_{\dot{w}} + mx_g)Z_{uu\delta_s} u^2 + (m - Z_{\dot{w}})M_{uu\delta_s} u^2},$$

$$d'_\theta = \frac{(M_{\dot{w}} + mx_g)d_w + (m - Z_{\dot{w}})d_q}{(M_{\dot{w}} + mx_g)Z_{uu\delta_s} u^2 + (m - Z_{\dot{w}})M_{uu\delta_s} u^2}. \tag{12}$$

Note that $m_\theta < 0$ because the conditions $(I_{yy} - M_{\dot{q}})(m - Z_{\dot{w}}) > (M_{\dot{w}} + mx_g)(Z_{\dot{q}} + mx_g)$, $Z_{uu\delta s} < 0$, and $Muu\delta_s < 0$ hold. Consequently, a positive elevator deflection generates a negative pitching moment, making the vehicle rotate clockwise.

Similarly, the pitch-tracking error θ_e is defined as $\theta_e = \theta - \theta_d$. The pitch-tracking error dynamic model can be written as

$$m_\theta \ddot{\theta}_e + d_\theta = \delta_s, \tag{13}$$

where d_θ denotes the combination of d'_θ and $m_\theta \ddot{\theta}_d$.

3.2. Transformed Depth-Tracking Kinematic Model

To derive a uniform second-order system from the depth-tracking kinematic model given in Equation (5), the following two assumptions are introduced [34,39,47].

Assumption 1. *The desired pitch angle θ_d described in Equation (7) can be precisely tracked by the pitch-tracking controller, i.e., $\theta \to \theta_d$.*

Assumption 2. *The attack angle α described in Equation (5) is slowly varying, which gives $\dot{\alpha} \approx 0$.*

Based on Assumption 1 and considering a constant desired depth z_d, inserting the desired pitch angle described in Equation (7) into the depth-tracking kinematic model defined in Equation (5) gives

$$\kappa \dot{z}_e + d_e z_e = \sin(\alpha - \hat{\alpha}), \tag{14}$$

where $d_e = \cos(\alpha - \hat{\alpha})/L$ denotes the damping coefficient, and κ is defined as $\kappa = \sqrt{z_e^2 + L^2}/(UL)$.

Based on Assumption 2, differentiating the depth-tracking kinematic model defined in Equation (14) with respect to time yields

$$m_z \ddot{z}_e + d_z = \dot{\hat{\alpha}}, \tag{15}$$

where

$$m_z = -\frac{\kappa}{\cos(\alpha - \hat{\alpha})}, \tag{16}$$

$$d_z = -\frac{\dot{\kappa}\dot{z}_e + \dot{d}_e z_e + d_e \dot{z}_e}{\cos(\alpha - \hat{\alpha})}. \tag{17}$$

It should be noted that we have $m_z < 0$ because the conditions $\kappa > 0$ and $\cos(\alpha - \hat{\alpha}) > 0$ hold. In this context, an increasing estimation of attack angle $\dot{\alpha}$ has the potential to produce negative depth-tracking acceleration $\ddot{z}_e$.

4. Uniform State-Constrained Response-Tunable Guidance and Control Framework

Since the pitch-tracking dynamic model in Equation (13) and the depth-tracking kinematic model in Equation (15) both conform to the uniform second-order system given in Equation (8), this section first develops a general control law to ensure the convergence of the tracking error ζ and then applies this uniform control framework to both the pitch-tracking and depth-tracking control tasks.

4.1. Uniform Control Law Design

As shown in Figure 3, a fourth-order polynomial planning trajectory

$$f(t) = a_0 + a_1 t + a_2 t^2 + a_3 t^3 + a_4 t^4, \tag{18}$$

can be uniquely determined to satisfy the following state constraints:

$$\begin{cases} f(0) = \zeta, \\ \dot{f}(0) = \dot{\zeta}, \end{cases} \tag{19}$$

$$\begin{cases} f(t_f) = 0, \\ \dot{f}(t_f) = 0, \\ \ddot{f}(t_f) = 0, \end{cases} \tag{20}$$

where $t = 0$ corresponds to the present sampling instant, and $t = t_f$ represents the future time at which the system states are expected to reach the setpoint.

In this context, the present polynomial planning acceleration can be calculated as

$$\ddot{f}(0) = 2a_2 = -\frac{6\dot{\zeta}}{t_f} - \frac{12\zeta}{t_f^2}. \tag{21}$$

To execute the present polynomial planning acceleration, the uniform control law is developed as

$$\tau = m_\zeta \ddot{f}(0) + \hat{d}_\zeta. \tag{22}$$

The uncertainty estimation is executed as

$$\hat{d}_\zeta = m_\zeta \hat{D}_\zeta, \tag{23}$$

$$\dot{\hat{D}}_\zeta = \sigma \ddot{f}(0), \tag{24}$$

where $\sigma \geq 0$ is an introduced integral gain.

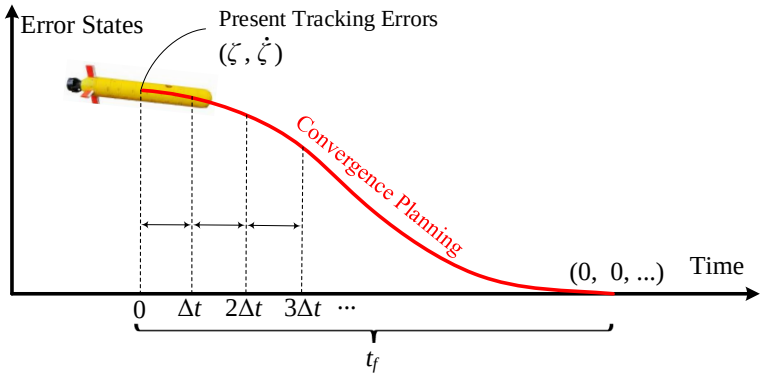


Figure 3. The AUV depth-tracking control block diagram.

4.2. Stability Analysis

Inserting the general control law defined in Equation (22) into the uniform second-order system given in Equation (8) yields

$$\ddot{\zeta} + \frac{6}{t_f}\dot{\zeta} + \frac{12}{t_f^2}\zeta + \frac{d_\zeta}{m_\zeta} - \hat{D}_\zeta = 0. \tag{25}$$

Substituting the uncertainty estimation given in Equations (23) and (24) into the above equation and then differentiating it with respect to time yields

$$\zeta^{(3)} + \frac{6}{t_f}\ddot{\zeta} + \left(\frac{12}{t_f^2} + \frac{6\sigma}{t_f}\right)\dot{\zeta} + \frac{12\sigma}{t_f^2}\zeta = n, \tag{26}$$

where n is defined as the derivative of d_ζ / m_ζ. The left-hand third-order polynomial is exponentially stable, as the inequality $(6/t_f)(12/t_f^2 + 6\sigma/t_f) > 12\sigma/t_f^2$ always holds. Consequently, the above second-order tracking system has bounded output states related to n. Moreover, the above error system is exponentially stable with a tunable convergence rate governed by t_f when the uncertainty term d_ζ varies slowly. It should be noted that this result does not imply finite-time convergence in the strict sense. When $n \approx 0$, the error system is exponentially stable with a convergence rate governed by t_f, whereas for $n < n_{\max}$ only ultimate boundedness can be guaranteed, and the residual bound depends on the magnitude of n. The distinction among finite-time convergence, exponential stability, and ultimate boundedness is thus clarified.

If n is not negligible, an error-state vector for (26) is defined as $\boldsymbol{X} = [\zeta, \dot{\zeta}, \ddot{\zeta}]^{\mathrm{T}}$. Its state-space form is represented as

$$\dot{\boldsymbol{X}} = \boldsymbol{A}\boldsymbol{X} + \boldsymbol{U}, \tag{27}$$

where

$$\boldsymbol{A} = \begin{bmatrix} 0 & 1 & 0 \\ 0 & 0 & 1 \\ -12\sigma/t_f^2 & -(12/t_f^2 + 6\sigma/t_f) & -6/t_f \end{bmatrix}, \tag{28}$$

$$\boldsymbol{U} = [0,\ 0,\ n]^{\mathrm{T}}. \tag{29}$$

The characteristic polynomial of $\boldsymbol{A}$ is the left-hand side of Equation (26). Thus, matrix $\boldsymbol{A}$ is Hurwitz for $\sigma > 0$ and $t_f > 0$. Since $\boldsymbol{A}$ is Hurwitz, the Lyapunov equation admits a unique positive definite solution $\boldsymbol{P}$ for any given positive definite $\boldsymbol{Q}$, which justifies the choice of the quadratic Lyapunov function $V = \boldsymbol{X}^{\mathrm{T}}\boldsymbol{P}\boldsymbol{X}$. Similar Lyapunov-based stability arguments have also been widely adopted in nonlinear control designs for engineering systems [46,48–50]. For a symmetric positive definite matrix $\boldsymbol{Q}$, there exists a unique symmetric positive definite matrix $\boldsymbol{P}$ satisfying the Lyapunov equation $\boldsymbol{A}^{\mathrm{T}}\boldsymbol{P} + \boldsymbol{P}\boldsymbol{A} = -\boldsymbol{Q}$ [50]. Taking its differentiation with respect to time gives

$$\dot{V} = -\boldsymbol{X}^{\mathrm{T}}\boldsymbol{Q}\boldsymbol{X} + 2\boldsymbol{X}^{\mathrm{T}}\boldsymbol{P}\boldsymbol{U}, \tag{30}$$

where the first term $-\boldsymbol{X}^{\mathrm{T}}\boldsymbol{Q}\boldsymbol{X}$ is negative definite and guarantees exponential stability of the nominal system, while the second term $2\boldsymbol{X}^{\mathrm{T}}\boldsymbol{P}\boldsymbol{U}$ is bounded by $2\|\boldsymbol{P}\|\|\boldsymbol{X}\|n_{\max}$ and ensures uniform ultimate boundedness under non-vanishing perturbations. Hence, $||\boldsymbol{X}|| \leq 2||\boldsymbol{P}||n_{max}/\lambda_{min}(\boldsymbol{Q})$ is the uniformly ultimately bound.

4.3. Pitch-Tracking Elevator Control Law Design

Based on the uniform control framework described above, the elevator control law that ensures the convergence of $\theta_e \to 0$ can be written as

$$\delta_s = m_\theta \ddot{\theta}_d + \hat{d}_\theta, \tag{31}$$

where the pitch-tracking polynomial planning desired acceleration $\ddot{\theta}_d$ and the nonlinear term estimation $\hat{d}_\theta$ are formulated as

$$\ddot{\theta}_d = -\frac{6}{t_\theta}\dot{\theta}_e - \frac{12}{t_\theta^2}\theta_e, \tag{32}$$

$$\hat{d}_\theta = m_\theta \hat{D}_\theta, \tag{33}$$

$$\dot{\hat{D}}_\theta = \sigma_\theta \ddot{\theta}_d, \quad \sigma_\theta \geq 0 \tag{34}$$

where t_θ is the pitch-tracking polynomial planning time duration.

4.4. Depth-Tracking Attack-Angle Update Law Design

Based on the transformed depth-tracking model in Equation (15), the update law for attack-angle estimation can be formulated as

$$\dot{\hat{\alpha}} = m_z \ddot{z}_d, \tag{35}$$

where the nonlinear term d_z is not included in the depth-tracking estimation, as it converges to zero together with the convergence of z_e and $\dot{z}_e$. The depth-tracking polynomial planning desired acceleration $\ddot{z}_d$ is formulated as

$$\ddot{z}_d = -\frac{6}{t_z}\dot{z}_e - \frac{12}{t_z^2}z_e, \tag{36}$$

where t_z is the depth-tracking polynomial planning time duration.

4.5. Slope-Filtering State Estimation

The AUV's position vector $\boldsymbol{\eta} = [x, y, z, \phi, \theta, \psi]^{\mathrm{T}}$ is measured by its onboard sensors. Let $\xi(t)$ denote one component of the AUV's position vector $\boldsymbol{\eta}$. Given that the nonlinear measured signal $\xi(t)$ can be linearized within a short time period [50], a slope-filtering technique based on statistical linear regression is developed to process this nonlinear signal over a selected time domain. Consider L pairs of sampled data, $(t_1, \xi(t_1))$, $(t_2, \xi(t_2))$, $\ldots$, $(t_k, \xi(t_k))$, $\ldots$, $(t_L, \xi(t_L))$, where k is an integer with $k \in [1, L]$, $t_1 < t_2 < \cdots < t_L$, and $\Delta t = t_k - t_{k-1}$ is the sampling interval. Note that $(t_L, \xi(t_L))$ corresponds to the measurement at the current instant, meaning the $L-1$ historical pairs $(t_1, \xi(t_1))$, $(t_2, \xi(t_2))$, $\ldots$, $(t_{L-1}, \xi(t_{L-1}))$ are taken as past observations. Hence, the filtered result of the present measured signal $\xi(t_L)$ is given by

$$\xi_f(t_L) = \rho + \mu_L t_L \tag{37}$$

where ρ and μ_L are calculated as

$$\mu_L = \frac{\sum_{k=1}^{L} \left(\xi(t_k) - \bar{\xi}\right)(t_k - \bar{t})}{\sum_{k=1}^{L} (t_k - \bar{t})^2}, \tag{38}$$

$$\rho = \bar{\xi} - \mu_L \bar{t}, \tag{39}$$

$\bar{\xi}$ represents the average of $\xi(t_k)$, and $\bar{t}$ denotes the average of t_k. In this case, ρ and μ_L are the filtered position and velocity of the measured signal $\xi(t)$, respectively. The larger the number of filtering length L, the better the denoising effects in the filtered position ρ and velocity μ_L. However, a larger filtering length L also increases the time lag, and vice versa. The measured signal $\xi(t)$ is assumed to be corrupted by zero-mean noise, and a larger L attenuates this noise more effectively but introduces a longer filtering delay of approximately $(L-1)\Delta t$. A higher sampling frequency reduces Δt and thus allows a larger L for the same tolerable delay, whereas a lower sampling frequency forces a smaller L to preserve the response speed. Therefore, L is chosen to balance noise suppression against filtering delay under the actual sampling frequency of the onboard sensors. The closed-loop block diagram for the depth-tracking control task is shown in Figure 4.

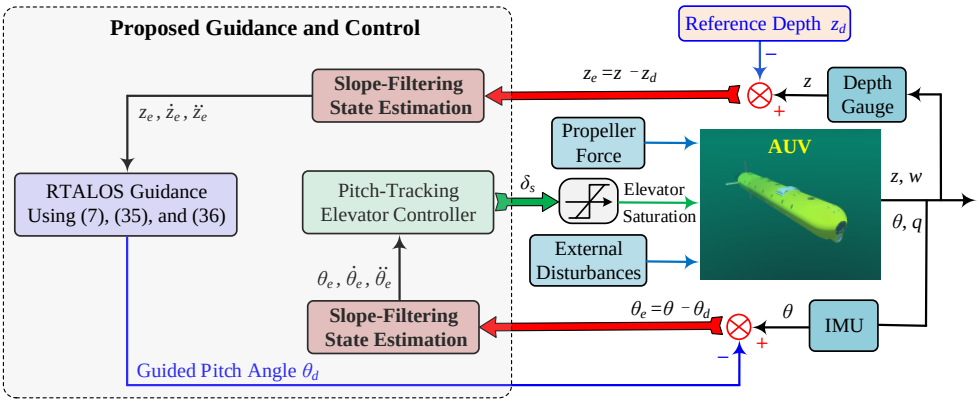


Figure 4. The AUV depth-tracking control block diagram.

5. Simulation Results

It should be clarified that the results presented in this section are obtained from a controller hardware-in-the-loop simulation rather than from field experiments. The AUV dynamics are numerically modeled, while the proposed guidance and control framework is executed on a real Raspberry Pi board. As shown in Figure 5, the Raspberry Pi acts as

the control unit and exchanges data with the ground station and the visualization engine through UDP communication over an industrial router. In this setup, the control algorithm runs on the Raspberry Pi with a fixed sampling period, and the AUV dynamics are solved with a simulation step sufficiently smaller than the sampling period to ensure numerical accuracy. The UDP communication delay between the control unit and the ground station is also small compared with the sampling period and therefore has a negligible effect on the depth-tracking performance. This confirms that the proposed framework can operate under realistic real-time constraints without a full-scale prototype.

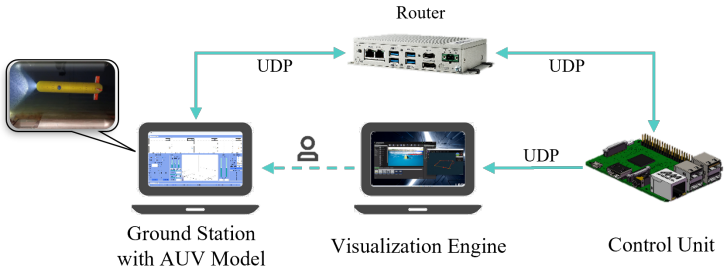


Figure 5. Hardware-in-the-loop simulation setup.

5.1. System Setup

The underactuated AUV prototype employed in the numerical simulation features a streamlined torpedo-shaped hull. Its profile is generated based on the Myring linear equation to reduce hydrodynamic resistance, as shown in Figure 6. The propulsion system consists of a 12 V brushless DC motor that directly drives the main propeller. It can deliver 70 N thrust at 3800 rpm, with a rated peak power of 180 W. A cruciform rudder configuration is mounted at the stern. The two horizontally arranged rudders are responsible for pitch motion control, while the two vertically arranged rudders are responsible for yaw motion control. The vehicle has a total length of 1.03 m and a diameter of 0.14 m. It consists of three independent pressure-tight compartments, with a certified operational depth of 300 m. The bow compartment is 0.11 m long and is used to carry mission payloads. The midship compartment is 0.74 m long and houses sensor arrays and electronic systems. The stern compartment is 0.18 m long and accommodates the propulsion system. The main parameters of the prototype are summarized in Table 2.

Regarding the guidance system parameters, the desired pitch angle is computed by Equation (7), while the attack-angle estimation is updated online according to Equations (35) and (36). The look-ahead distance is set to $L = 2.7$ m, and the attack-angle estimation parameter is set to $m_z = -5$. The finite planning time is configured as $t_z = 3$ s, $t_z = 6$ s, and $t_z = 9$ s, respectively, to investigate the dependence of the depth-tracking convergence time on the preset planning time; i.e., a larger planning time leads to slower convergence. The pitch-tracking control parameters are set according to Equations (31)–(34), with $m_\theta = -5$, $\sigma_\theta = 0.03$, and $t_\theta = 3$ s. Here, $t_\theta < t_z$ is enforced to ensure that the depth-tracking response is slower than the pitch-tracking control, thereby guaranteeing timely and accurate pitch tracking [22].

The tuning of the proposed guidance and control scheme is straightforward, since the response of the closed-loop system is mainly governed by the planning-time parameters rather than by a large number of feedback gains. Specifically, t_θ determines the convergence rate of the pitch-tracking loop, while t_z determines the convergence rate of the depth-tracking loop, and the only constraint required for tuning is $t_\theta < t_z$. The remaining parameters, namely m_z, m_θ, and σ_θ, can be determined directly from the physical characteristics of the AUV system. Consequently, these parameters can be computed rather than tuned by trial and error, which further reduces the tuning effort of the proposed scheme. To evaluate the active disturbance rejection capability of the RTALOS method

under time-varying large-amplitude load disturbances, the external disturbance applied in the heave direction is defined as

$$d_w(t) = \begin{cases} 0, & 0 \le t < 50, \\ 0.08W \sin\left(2\pi \cdot 0.03\,(t-50)\right), & 50 \le t < 100, \\ 0.08W, & t \ge 100, \end{cases}$$

where W denotes the vehicle weight.

To verify the response-tunable convergence property of the proposed RTALOS guidance, three comparative tests are designed: (1) $t_z = 3$ s and $t_\theta = 2.5$ s; (2) $t_z = 6$ s and $t_\theta = 2.5$ s; (3) $t_z = 9$ s and $t_\theta = 2.5$ s, where a larger t_z results in slower depth convergence. The desired depth is fixed at 3 m. To comprehensively evaluate the performance of different guidance and control strategies, five comparative scenarios are established: (1) Proposed Control + Proposed Guidance; (2) PD Control + Proposed Guidance; (3) ADRC + Proposed Guidance; (4) Proposed Control + ALOS Guidance; (5) Proposed Control + ILOS Guidance.

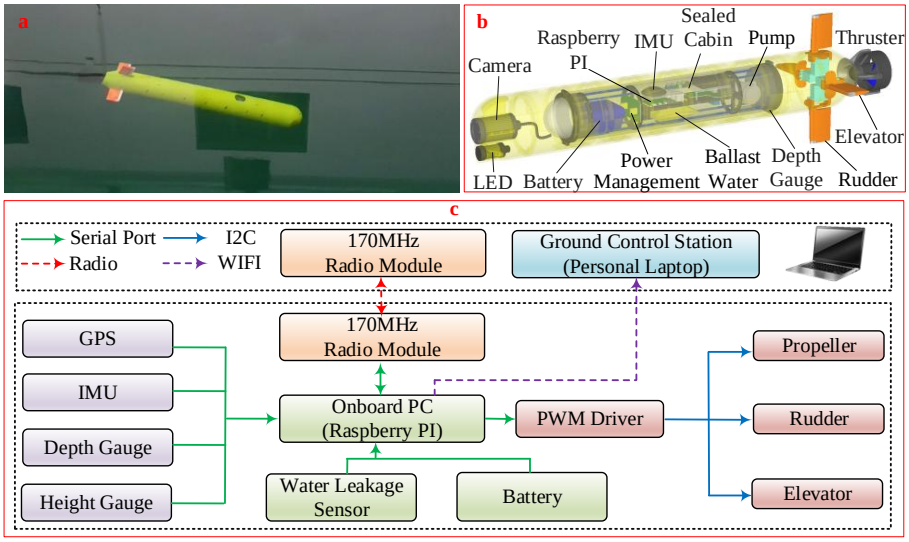


Figure 6. The underactuated AUV prototype used in numerical simulations. (**a**) AUV prototype in towing tank; (**b**) AUV Components; (**c**) Hardware connection.

Table 2. Main features of the AUV prototype.

Parameters	Descriptions	Values
m	AUV mass	8.25 kg
L_{oa}	AUV length	1.03 m
D	AUV diameter	0.14 m
W	AUV gravity	80.85 N
B	AUV buoyancy	82.85 N
I_{xx}	Inertial moment about x axis	0.0258 kg·m^2
I_{yy}	Inertial moment about y axis	0.508 kg·m^2
I_{zz}	Inertial moment about z axis	0.508 kg·m^2
D_p	Propeller diameter	0.06 m
τ	Maximum force	70 N

5.2. Main Results

To verify the response-tunable convergence property of the proposed RTALOS guidance, three comparative tests were designed. The preset planning time of the pitch-tracking controller was uniformly set to $t_\theta = 2.5$ s. Since the control input of the derived second-order kinematic model for the depth-tracking error is the first derivative of the attack-angle

estimation, i.e., $\hat{\dot{\alpha}}$, the preset planning time for the attack-angle estimation was configured as $t_z = 3$ s, $t_z = 6$ s, and $t_z = 9$ s, respectively. The corresponding simulation results are presented in Figure 7. The first two subplots correspond to the depth and its velocity, respectively, which are exactly the basis for computing the first derivative of the attack-angle estimate, as calculated by Equation (35). The estimation $\hat{\dot{\alpha}}$ given in subplot 3 is then updated online through Equation (36) to obtain the attack-angle estimation present in subplot 4. Based on the attack-angle estimation results, the desired pitch angle is calculated by Equation (7) shown in subplot 5. As observed from the simulation results, the scenario with $t_z = 3$ s converges after approximately 25 s, while the scenario with $t_z = 9$ s converges after about 45 s, indicating that the convergence time increases with larger t_z. A time-varying load is added onto the vehicle rigid body after 50 s. A comprehensive comparison shows that the scenario with $t_z = 3$ s achieves the highest tracking accuracy (maximum deviation of about 3 cm), while the scenario with $t_z = 9$ s exhibits the largest deviation (about 15 cm). From the analysis of the attack-angle estimation results shown in subplot 4, the scenario with $t_z = 3$ s responds the fastest, whereas the scenario with $t_z = 9$ s responds the slowest. This is because a smaller t_z leads to a larger planned acceleration $\ddot{z}_d$ in Equation (36). It should be noted that a smaller t_z is not always better, as its lower bound is constrained by the pitch-tracking planning time $t_\theta = 2.5$ s. Therefore, $t_z = 3$ s is selected in this paper. The guidance gain is tuned to achieve a smooth depth response, while the pitch-loop gains are chosen such that the pitch-tracking response is faster than the guidance response; i.e., $t_\theta < t_z$, so that the desired pitch angle is tracked in time. Since a larger t_z leads to a slower guidance response, t_z is selected only larger than t_θ.

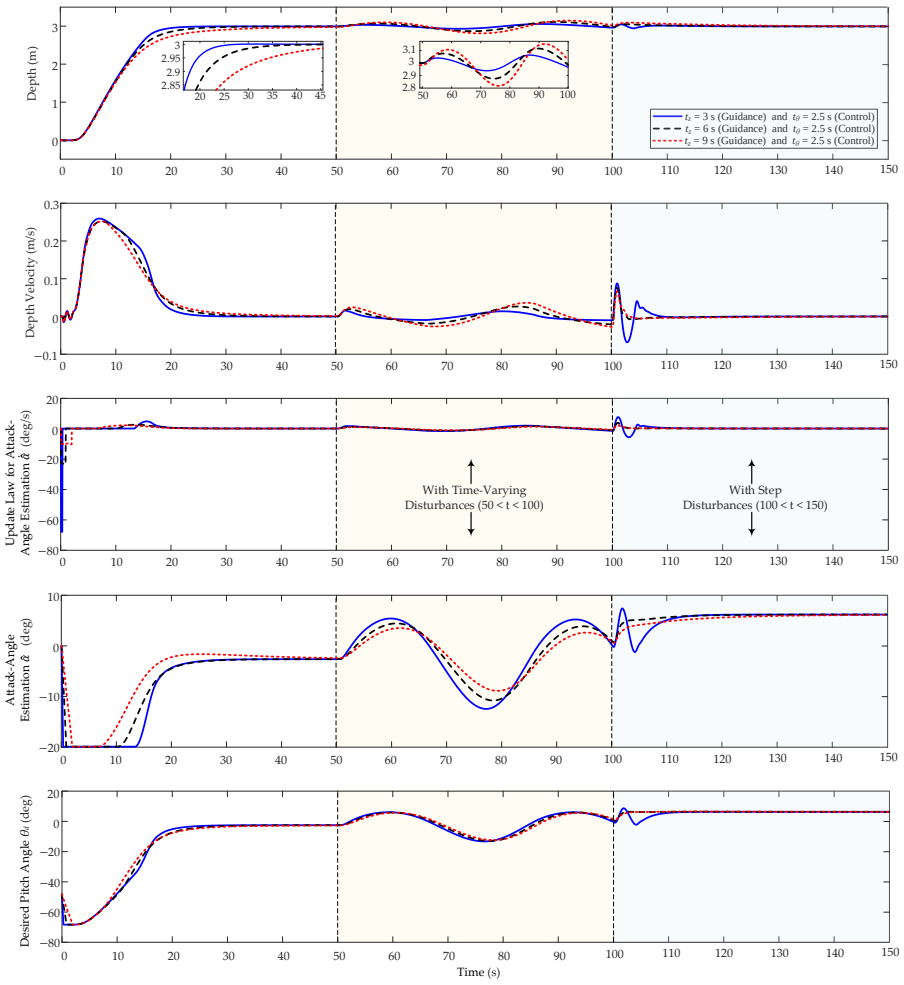


Figure 7. The AUV depth-tracking results with the proposed RTALOS guidance.

After obtaining the desired pitch angle, it is necessary for the pitch-tracking tracking controller to achieve fast and accurate tracking performance. The results are shown in Figure 8. This figure sequentially presents the pitch angle, pitch-tracking error, its velocity, nonlinear term estimation calculated by Equations (33) and (34), and the elevator angle. From the tracking error given in subplot 3, it can be observed that under the condition of $t_\theta = 2.5$ s, the pitch angle achieves convergence before 20 s, which is faster than the scenario convergence around 25 s with $t_z = 3$ s. After the time-varying load is applied at 50 s, the nonlinear term estimation in subplot 4 maintains fast and accurate pitch-tracking performance, and the pitch-tracking error in subplot 3 is approximately 1° at maximum, which verifies the robustness of the proposed pitch-tracking controller.

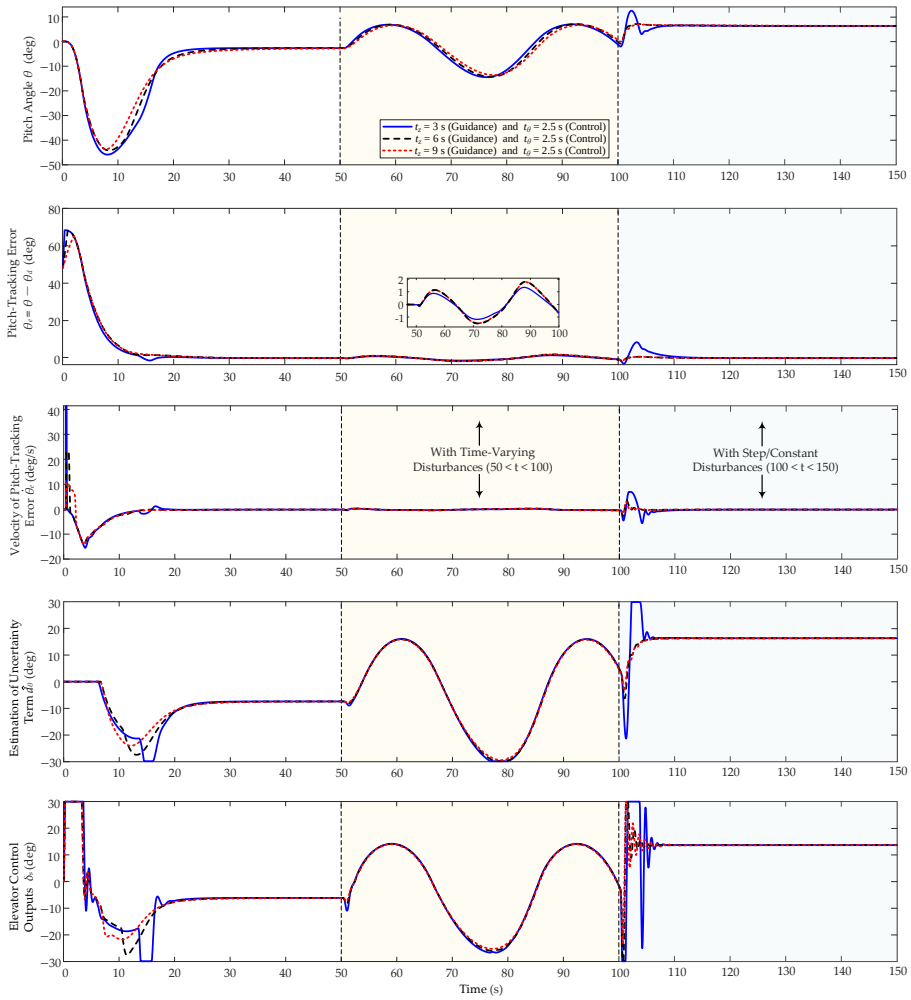


Figure 8. The pitch-tracking results with the proposed controller.

To verify the superiority of the RTALOS guidance, five scenarios of comparative tests were designed. The first three scenarios pair the RTALOS guidance with PD, ADRC, and the proposed controller, respectively, to examine its adaptability when cascaded with different controllers. The last two scenarios pair the proposed controller with ILOS and ALOS guidance, respectively, to verify its robustness relative to other guidance algorithms under time-varying external disturbances. Figure 9 presents seven subplot results, including the depth, attack-angle estimate, desired pitch angle, actual pitch angle, pitch-tracking error, nonlinear term estimation for pitch tracking, and elevator angle. A comprehensive analysis of the simulation data after 50 s is presented in Table 3, which includes the mean absolute error (AAE $= \frac{1}{N}\sum_{i=1}^{N}|e_i|$), the standard deviation of error (SDE $= \sqrt{\frac{1}{N}\sum_{i=1}^{N}(e_i - \bar{e})^2}$), the maximum absolute error (MAE $= \max(|e_i|)$), the integral

of absolute control input (IACI $= \int_0^T |u(t)|\,\mathrm{d}t$), and the standard deviation of control input (SDCI $= \sqrt{\frac{1}{N}\sum_{i=1}^{N}(u_i - \bar{u})^2}$). It can be seen that the RTALOS guidance performs excellently when paired with different controllers. Notably, under PD control (black dashed line), although the pitch-tracking error given in subplot 5 exhibits significant oscillation, this deviation is promptly compensated in the attack-angle estimation, and the depth-tracking result still remains satisfactory. In contrast, both the ILOS and ALOS guidance methods rely on the integral of depth-tracking error to estimate the attack angle, resulting in sluggish changes in the attack-angle estimation and insufficient disturbance rejection capability under time-varying external disturbances. This leads to abnormal oscillations in depth-tracking results, with a maximum deviation of approximately 40 cm. In summary, the five scenarios of comparative tests validate the adaptability of the proposed RTALOS guidance to different controllers and its superiority over existing ILOS and ALOS guidance methods.

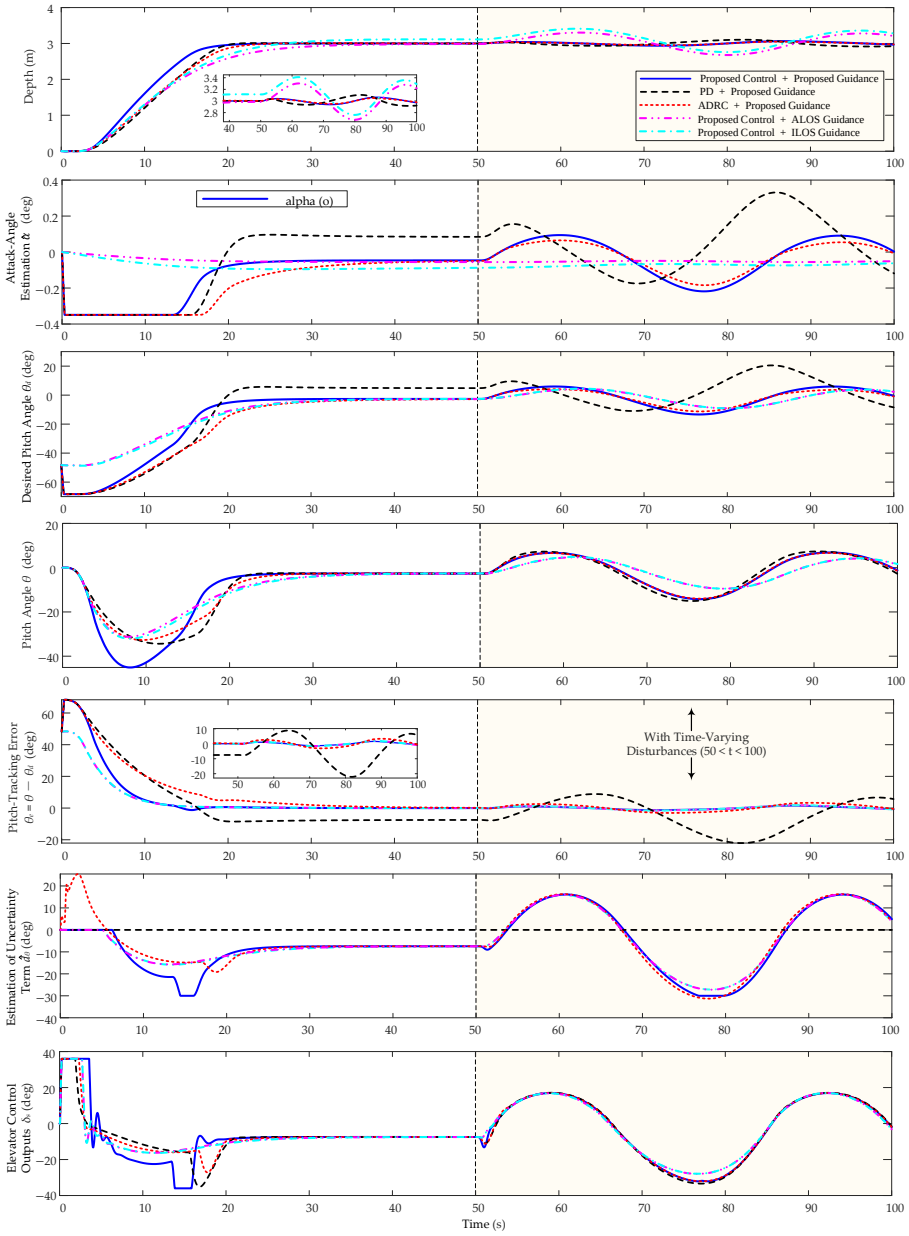


Figure 9. The comparative results among selected guidance and control methods.

Table 3. Comparisons of depth-tracking performance across selected methods for 50 s $< t <$ 100 s.

Comparative Methods	Depth-Tracking Guidance			Pitch-Tracking Control				
	AAE (m)	SDE (m)	MAE (m)	AAE (deg)	SDE (deg)	MAE (deg)	IACI (deg·t)	SDCI (deg)
Proposed Control + Proposed Guidance	0.034	0.038	0.064	0.739	0.851	1.538	754.8	17.31
PD + Proposed Guidance	0.052	0.060	0.104	8.769	10.01	8.845	775.6	17.79
ADRC + Proposed Guidance	0.037	0.041	0.070	1.878	2.096	3.322	759.8	17.34
Proposed Control + ALOS Guidance	0.232	0.215	0.411	0.895	1.024	1.820	708.3	16.87
Proposed Control + ILOS Guidance	0.191	0.209	0.302	0.897	1.027	1.822	710.2	16.91

6. Conclusions

This paper proposed an RTALOS guidance law for the depth-tracking control of underactuated AUVs. Unlike the existing ILOS and ALOS guidance approaches that solely employed the integral actions of the depth-tracking error, the proposed RTALOS guidance incorporated both the depth-tracking error and its first-order derivative into the attack-angle estimation, establishing a second-order kinematic framework for guidance design. The first-order derivative term served as an adjustable damping mechanism, which could effectively suppress the overshoot and oscillation effects inherently caused by pure integral operations. Moreover, by generating the desired acceleration through a time-based planning polynomial with state constraints, the proposed guidance law endowed the depth-tracking system with response-tunable convergence characteristics, where the convergence time could be prescribed in advance via the planning-time parameter. Simulation results demonstrated that the proposed RTALOS guidance successfully achieved response-tunable depth convergence with significantly reduced overshoot and chattering. Furthermore, the results showed that even when the low-level pitch-tracking control was realized by a simple PD controller, the proposed attack-angle estimation could promptly and accurately compensate for time-varying disturbances and pitch-control deviations, enabling outstanding depth-tracking accuracy under severe time-varying external loads.

Nevertheless, several limitations remain. The proposed RTALOS guidance has been validated only through controller hardware-in-the-loop simulations, and its performance under real ocean environments has not been experimentally verified. In addition, the coupling between attack-angle and sideslip-angle compensation in three-dimensional path following has not been addressed. Further investigation will be directed toward experimental validation using the prototype AUV described in this paper to assess the practical applicability of the proposed RTALOS guidance, as well as the extension of the current framework to three-dimensional spatial path following with simultaneous attack-angle and sideslip-angle compensation.

Author Contributions: Conceptualization, methodology and software, Y.Q., C.N. and Z.Y.; data curation and validation, G.W., S.Z. and W.H.; writing and editing, X.L.; supervision and funding acquisition, Y.Q. All authors have read and agreed to the published version of the manuscript.

Funding: This research was funded by the Hubei Technology Innovation Center for Smart Hydropower under Grant No. HBCXZX-JJ-202411.

Data Availability Statement: The original contributions presented in this study are included in the article. Further inquiries can be directed to the corresponding author.

Acknowledgments: The authors would like to thank the reviewers for their constructive comments.

Conflicts of Interest: Authors Mr. Xinyu Li, Mr. Gang Wan and Mr. Sisi Zhu were employed by the company "Hubei Technology Innovation Center for Smart Hydropower". The remaining authors declare that the research was conducted in the absence of any commercial or financial relationships

that could be construed as a potential conflict of interest. The authors declare that this study received funding from Hubei Technology Innovation Center for Smart Hydropower. The funder was not involved in the study design, collection, analysis, interpretation of data, the writing of this article or the decision to submit it for publication.

Abbreviations

The following abbreviations are used in this manuscript:

AUVs	Autonomous underwater vehicles
LOS	Line-of-sight
ILOS	Integral line-of-sight
ALOS	Adaptive line-of-sight
RTALOS	Response-tunable adaptive line-of-sight
ADRC	Active disturbance rejection control
PD	Proportional-derivative
AAE	Mean absolute error
SDE	Standard deviation of error
MAE	Maximum absolute error
IACI	Integral of absolute control input
SDCI	Standard deviation of control input

References

1. Fang, K.; Fang, H.; Zhang, J.; Yao, J.; Li, J. Neural adaptive output feedback tracking control of underactuated AUVs. *Ocean Eng.* **2021**, *234*, 109211. [CrossRef]
2. Xiang, X.; Yu, C.; Zhang, Q. Robust fuzzy 3D path following for autonomous underwater vehicle subject to uncertainties. *Comput. Oper. Res.* **2017**, *84*, 165–177. [CrossRef]
3. Li, D.; Du, L. AUV Trajectory Tracking Models and Control Strategies: A Review. *J. Mar. Sci. Eng.* **2021**, *9*, 1020. [CrossRef]
4. Yang, Y.; Xiao, Y.; Li, T. A Survey of Autonomous Underwater Vehicle Formation: Performance, Formation Control, and Communication Capability. *IEEE Commun. Surv. Tutor.* **2021**, *23*, 815–841. [CrossRef]
5. Bian, Y.; Cheng, J.; Du, C.; Hu, M.; Cui, Q.; Ding, R. A hierarchical framework for finite-time cooperative depth control of heterogeneous multi-AUV system. *Ocean Eng.* **2024**, *308*, 117976. [CrossRef]
6. Yuan, C.; Shuai, C.; Ma, J. A Novel Real-Time Obstacle Avoidance Method in Guidance Layer for AUVs' Path Following. *IEEE Trans. Veh. Technol.* **2024**, *73*, 1845–1856. [CrossRef]
7. Patil, P.V.; Khan, M.K.; Korulla, M.; Nagarajan, V.; Sha, O.P. Design optimization of an AUV for performing depth control maneuver. *Ocean Eng.* **2022**, *266*, 112929. [CrossRef]
8. Lin, Y.H.; Yu, C.M.; Wu, I.C.; Wu, C.Y. The depth-keeping performance of autonomous underwater vehicle advancing in waves integrating the diving control system with the adaptive fuzzy controller. *Ocean Eng.* **2023**, *268*, 113609. [CrossRef]
9. Ahmed, F.; Xiang, X.; Jiang, C.; Xiang, G.; Yang, S. Survey on traditional and AI based estimation techniques for hydrodynamic coefficients of autonomous underwater vehicle. *Ocean Eng.* **2023**, *268*, 113300. [CrossRef]
10. Cho, G.R.; Kang, H.; Kim, M.G.; Lee, M.J.; Li, J.H.; Kim, H.; Lee, H.; Lee, G. An Experimental Study on Trajectory Tracking Control of Torpedo-like AUVs Using Coupled Error Dynamics. *J. Mar. Sci. Eng.* **2023**, *11*, 1334. [CrossRef]
11. Kim, K.; Sato, T.; Oono, A.Z Depth-based pseudo-terrain-following navigation for cruising AUVs. *Control Eng. Pract.* **2023**, *131*, 105379. [CrossRef]
12. Guo, L.; Sun, X.; Chen, H.; Wang, F. Coupled depth-pitch control of AUVs using hierarchical adaptive backstepping under ocean environmental disturbances. *Ships Offshore Struct.* **2025**, 1–23. [CrossRef]
13. Wang, J.; Yan, S.; Bao, H.; Chen, C.; Yu, D.; Li, J.; Chen, X.; Dou, R.; Tang, Y.; Li, S. Reinforcement-Learning-Based Adaptive PID Depth Control for Underwater Vehicles Against Buoyancy Variations. *J. Mar. Sci. Eng.* **2026**, *14*, 323. [CrossRef]
14. Li, J.; Xiang, X.; Dong, D.; Yang, S. Prescribed time observer based trajectory tracking control of autonomous underwater vehicle with tracking error constraints. *Ocean Eng.* **2023**, *274*, 114018. [CrossRef]
15. Jiang, Z.; Wang, Z.; Li, P.; Qin, H. Ground effect modeling and dynamic response analysis of a subsea autonomous underwater vehicle near seabed with terrain. *Phys. Fluids* **2025**, *37*. [CrossRef]
16. Xu, Y.; Wan, L.; Qin, H.; Miao, J.; Zhu, C. Rotation matrix-based finite-time trajectory tracking control of benthic AUV with communication bandwidth limitation. *J. Vib. Control* **2026**, *32*, 716–734. [CrossRef]

17. Liu, C.; Xiang, X.; Duan, Y.; Yang, L.; Yang, S. ADRC-SMC-based disturbance rejection depth-tracking control of underactuated AUV. *J. Field Robot.* **2024**, *41*, 1103–1115. [CrossRef]
18. Wang, W.; Yi, Y.; Wang, Q.; Yang, J.; Yu, J. Intermittent information-based disturbance observer design and recursive depth control for AUVs with packet losses. *IEEE Trans. Circuits Syst. I Regul. Pap.* **2025**, *72*, 7346–7357. [CrossRef]
19. Tajudeen, M.M.; Banu, K.A.; Tatar, N.e.; Contreras, R.C.; Rajchakit, G.; Akgül, A. Observer-based secure control for networked control systems with multiple disturbances, actuator failures, and deception attacks under adaptive event-triggered mechanism: MM Tajudeen et al. *Sci. Rep.* **2026**, *16*, 10092. [PubMed]
20. He, X.; Dong, S.; Liu, E.; Wu, Z.G.; Liu, M.; Wang, H. Fault-Tolerant Dynamic Periodic Event-Based Depth Control of AUVs With Prescribed-Time Observer. *IEEE Control Syst. Lett.* **2026**, *10*, 91–96. [CrossRef]
21. Tajudeen, M.M.; Banu, K.A.; Manoj, K.; Rajchakit, G.; Abdalla, M.; Huang, T. Secure observer-based event-triggered sliding mode control for complex networks under deception attacks. *J. Frankl. Inst.* **2026**, *363*, 108517. [CrossRef]
22. Qu, Y.; Zhang, Q.; Xiang, X.; Yang, S.; Cai, L. Cascaded guidance, state estimation, and control for depth tracking of underactuated autonomous underwater vehicles. *Commun. Eng.* **2025**, *4*, 191. [CrossRef] [PubMed]
23. Lekkas, A.M.; Fossen, T.I. Integral LOS Path Following for Curved Paths Based on a Monotone Cubic Hermite Spline Parametrization. *IEEE Trans. Control Syst. Technol.* **2014**, *22*, 2287–2301. [CrossRef]
24. Fossen, T.I.; Pettersen, K.Y. On uniform semiglobal exponential stability (USGES) of proportional line-of-sight guidance laws. *Automatica* **2014**, *50*, 2912–2917. [CrossRef]
25. Rout, R.; Subudhi, B. Design of Line-of-Sight Guidance Law and a Constrained Optimal Controller for an Autonomous Underwater Vehicle. *IEEE Trans. Circuits Syst. II Express Briefs* **2021**, *68*, 416–420. [CrossRef]
26. Gu, N.; Wang, D.; Peng, Z.; Wang, J.; Han, Q.L. Advances in Line-of-Sight Guidance for Path Following of Autonomous Marine Vehicles: An Overview. *IEEE Trans. Syst. Man Cybern. Syst.* **2023**, *53*, 12–28. [CrossRef]
27. He, L.; Zhang, Y.; Fan, G.; Liu, Y.; Wang, X.; Yuan, Z. Three-dimensional path following control of underactuated AUV based on nonlinear disturbance observer and adaptive line-of-sight guidance. *IEEE Access* **2024**, *12*, 83911–83924. [CrossRef]
28. Zhang, Y.; Li, S.; Wang, W.; Wang, S.; Mu, R. Three-dimensional path following control of underactuated autonomous underwater vehicles with nonzero roll dynamics: A novel line-of-sight-guided approach. *Int. J. Robust Nonlinear Control* **2024**, *34*, 4959–4977. [CrossRef]
29. Fossen, T.I.; Aguiar, A.P. A uniform semiglobal exponential stable adaptive line-of-sight (ALOS) guidance law for 3-D path following. *Automatica* **2024**, *163*, 111556. [CrossRef]
30. Wu, W.; Peng, Z.; Wang, D.; Liu, L.; Han, Q.L. Network-Based Line-of-Sight Path Tracking of Underactuated Unmanned Surface Vehicles With Experiment Results. *IEEE Trans. Cybern.* **2022**, *52*, 10937–10947. [CrossRef] [PubMed]
31. Yang, G.; Li, L.; Zhang, K.; Liu, W. Lyapunov-based model predictive control for path-following of an autonomous underwater vehicle using line-of-sight guidance. *Mechatronics* **2026**, *115*, 103464. [CrossRef]
32. Qu, Y.; Cai, L. Nonlinear positioning control for underactuated unmanned surface vehicles in the presence of environmental disturbances. *IEEE/ASME Trans. Mechatron.* **2022**, *27*, 5381–5391. [CrossRef]
33. Qu, Y.; Cai, L. An adaptive delay-compensated filtering system and the application to path following control for unmanned surface vehicles. *ISA Trans.* **2023**, *136*, 548–559. [CrossRef] [PubMed]
34. Fossen, T.I. An Adaptive Line-of-Sight (ALOS) Guidance Law for Path Following of Aircraft and Marine Craft. *IEEE Trans. Control Syst. Technol.* **2023**, *31*, 2887–2894. [CrossRef]
35. Yu, C.; Liu, C.; Lian, L.; Xiang, X.; Zeng, Z. ELOS-based path following control for underactuated surface vehicles with actuator dynamics. *Ocean Eng.* **2019**, *187*, 106139. [CrossRef]
36. Liu, L.; Wang, D.; Peng, Z.; Wang, H. Predictor-based LOS guidance law for path following of underactuated marine surface vehicles with sideslip compensation. *Ocean Eng.* **2016**, *124*, 340–348. [CrossRef]
37. Liu, L.; Wang, D.; Peng, Z. ESO-based line-of-sight guidance law for path following of underactuated marine surface vehicles with exact sideslip compensation. *IEEE J. Ocean. Eng.* **2017**, *42*, 477–487. [CrossRef]
38. Du, P.; Yang, W.; Chen, Y.; Huang, S.H. Improved indirect adaptive line-of-sight guidance law for path following of under-actuated AUV subject to big ocean currents. *Ocean Eng.* **2023**, *281*, 114729. [CrossRef]
39. Fossen, T.I.; Pettersen, K.Y.; Galeazzi, R. Line-of-Sight Path Following for Dubins Paths With Adaptive Sideslip Compensation of Drift Forces. *IEEE Trans. Control Syst. Technol.* **2015**, *23*, 820–827. [CrossRef]
40. Caharija, W.; Pettersen, K.Y.; Bibuli, M.; Calado, P.; Zereik, E.; Braga, J.; Gravdahl, J.T.; Sørensen, A.J.; Milovanović, M.; Bruzzone, G. Integral Line-of-Sight Guidance and Control of Underactuated Marine Vehicles: Theory, Simulations, and Experiments. *IEEE Trans. Control Syst. Technol.* **2016**, *24*, 1623–1642. [CrossRef]
41. Duan, Y.; Xiang, X.; Liu, C.; Yang, L. Double-loop LQR depth tracking control of underactuated AUV: Methodology and comparative experiments. *Ocean Eng.* **2024**, *300*, 117410. [CrossRef]
42. Xiong, X.; Xiang, X.; Duan, Y.; Yang, S. Adaptive SNDO-STSM Hierarchical Robust Control of Autonomous Underwater Vehicle: Theory and Experimental Validation. *IEEE Trans. Ind. Electron.* **2024**, *71*, 14351–14361. [CrossRef]

43. Li, X.; Qin, H.; Guo, Z.; Xue, Y. Adaptive fixed-time fault-tolerant fuzzy control of AUVs with asymmetric output constraints. *IET Intell. Transp. Syst.* **2024**, *18*, 2034–2048. [CrossRef]
44. Xu, Y.; Zhang, Z.; Wan, L. Robust prescribed-time ESO-based practical predefined-time SMC for benthic AUV trajectory-tracking control with uncertainties and environment disturbance. *J. Mar. Sci. Eng.* **2024**, *12*, 1014. [CrossRef]
45. Qu, Y.; Cai, L.; Xu, H. Curved path following for unmanned surface vehicles with heading amendment. *IEEE Trans. Syst. Man Cybern. Syst.* **2021**, *51*, 4183–4192. [CrossRef]
46. Fossen, T.I. *Handbook of Marine Craft Hydrodynamics and Motion Control*; John Wiley & Sons: Hoboken, NJ, USA, 2011.
47. Fossen, T.I.; Lekkas, A.M. Direct and indirect adaptive integral line-of-sight path-following controllers for marine craft exposed to ocean currents. *Int. J. Adapt. Control Signal Process.* **2017**, *31*, 445–463. [CrossRef]
48. Adil, H.M.M.; Ahmed, S.; Ahmad, I. Control of MagLev System Using Supertwisting and Integral Backstepping Sliding Mode Algorithm. *IEEE Access* **2020**, *8*, 51352–51362. [CrossRef]
49. Adil, H.M.M.; Khan, H.A. WOA-tuned supertwisted synergetic control of multipurpose on-board charger for G2V/V2G/V2V operational modes of electric vehicles. *Control Eng. Pract.* **2025**, *154*, 106136. [CrossRef]
50. Khalil, H.K. *Nonlinear Systems*, 3rd ed.; Prentice Hall: Saddle River, NJ, USA, 2001.

Disclaimer/Publisher's Note: The statements, opinions and data contained in all publications are solely those of the individual author(s) and contributor(s) and not of MDPI and/or the editor(s). MDPI and/or the editor(s) disclaim responsibility for any injury to people or property resulting from any ideas, methods, instructions or products referred to in the content.